Topics in Current Chemistry (2004) 246: 15–31
DOI 10.1007/b98647

New Horizons for Magic-Angle Spinning NMR

Ago Samoson (✉) · Tiit Tuherm · Jaan Past · Andres Reinhold · Tiit Anupõld · Ivo Heinmaa

National Institute of Chemical Physics and Biophysics, Akadeemia Tee 23, Tallinn Estonia
ago@kbfi.ee

Abstract Recent developments in sample rotation technology have had a profound impact on magic-angle-spinning NMR. First, rotation frequencies approaching, and even exceeding, strong homonuclear spin interactions have made high-resolution solid-state ^{1}H spectroscopy much more accessible. Second, the new concept of fast rotation sweep spectroscopy has emerged. Third, high-resolution NMR at cryogenic temperatures has become feasible, offering an enormous sensitivity gain and the opportunity to study a wide range of physical phenomena.

Keywords Magic-Angle Spinning NMR · Sample rotation · Rotor size · Selectivity · Sensitivity · Spectral resolution

1 Introduction

Magic-angle-spinning (MAS) NMR is one of the most fascinating experimental techniques in modern science, offering unprecedented cross-disciplinary applications. MAS NMR, with rotors routinely spinning at subsonic rates, is being used across the world by physicists, chemists, biologists and materials scientists. Although the technique was invented in the late 1950s, it became widely used only about 25 years later, due to advances in spectrometer hardware and ceramics technology. The sample spinning systems now use much more stable double-

bearing designs than the prototype mushroom-shaped Andrew-Beams rotors. The rotors are fixed in a shaft by gas-lubricated bearings, while the driving momentum is provided by one or more separate sets of high speed gas jets.

Originally designed with the aim of eliminating internuclear interactions, MAS spectroscopy was concerned with a systematic study of cross-polarization between abundant and rare spin systems. Subsequent developments have introduced many sophisticated manipulations of spin interactions to unravel the structure and dynamics of solid materials. The latest advances described in this contribution illustrate the new methods of tackling the problems of selectivity, sensitivity and spectral resolution.

2 Basic Theory

The product of maximum sustained rotation frequency and rotor diameter, obtained from the well-known relationship

$$\nu = \frac{\sqrt{3}}{\pi} \sqrt{\frac{T\Delta}{\varrho}} \frac{1}{D}$$

where T is the tensile strength of the material, Δ the relative wall thickness of the rotor, ϱ density of the material and D the rotor diameter, is at present ~90 Hz m, so that the external surface of the rotor travels at ca. 85% of the speed of sound. The actual limit depends primarily on the tensile strength of the rotor material, provided that the necessary precautions concerning rotor balancing and bearing lubrication are taken [1].

Not only the ultimate speed but also the safety of operation are very important considerations in MAS NMR. For example, isotopically labelled biopolymers are not only very expensive, but may also pose a serious health hazard if a rotor containing a sample such as amyloid fibril protein disintegrates in the laboratory.

Reliable operation of MAS requires a reasonable understanding of the principles of mechanics, careful rotor handling and a stable supply of very clean compressed gas. The performance and stability of the experiment depend on the quality of rotor filling, which can be conveniently tested by a histogram of the rotor speed. The alignment of the rotor with respect to its bearings can be described in terms of harmonic oscillations. To a good approximation, the deviation of the axis of the rotor from the ideal position is countered by a force proportional to the deviation at low spinning frequencies. The rotor then experiences two mechanical resonances, characteristic of translational and conical whirl modes, at the respective frequencies

$$\omega_{\mathrm{T}} = \sqrt{\frac{2K}{M}} \tag{1}$$

$$\omega_C = \sqrt{\frac{K}{2(I_\perp - I_A)}} L_B \tag{2}$$

where K is the bearing force constant and L_B is the length of the bearing. Transverse and axial inertial moments depend on the diameter, length and mass of the rotor:

$$I_\perp = \left(\frac{D^2}{16} + \frac{L^2}{12}\right) M \tag{3}$$

$$I_A = \frac{D^2}{8} M \tag{4}$$

The frequency of the conical resonance is ca. 1.4 times higher than the translational resonance for a typical aspect ratio $a=L/D$ of the rotor. Demand for the rotor drive energy increases on approaching the mechanical resonance frequency. The increasing amplitude of the rotor deviation from the symmetry axis on approaching the frequency of mechanical resonance directs part of the drive energy to vibration of the rotor housing. Figure 1 shows a set of rotation speed spectrograms for different bearing pressures, with a slow gradual in-

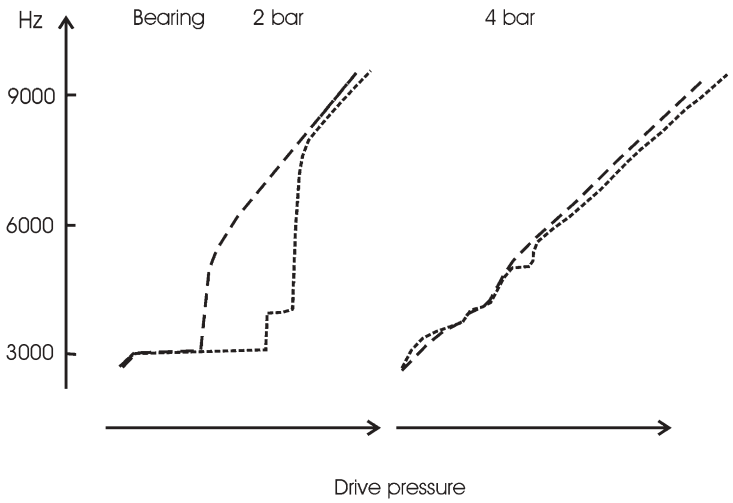

Fig. 1 Mechanical resonances of a 4-µL rotor filled with a specially shaped solid, simulating cylindrical and conical asymmetry. Rotation speed was slowly increased by servo-controlled drive pressure. Cylindrical imbalance (*long dash*) enables corresponding modes of resonance to be identified. The ratio of jerk positions closely corresponds to the theoretical ratio of two different resonance modes. Higher bearing pressure increases the force constant and the frequencies of the mechanical resonances

crease in the drive pressure. The mechanical resonance parameters can be readily identified by using a test rotor with deliberately simulated asymmetric rotor filling. The increase in rotor speed almost disappears on approaching the resonance condition. After passing the resonance threshold, the rotor picks up speed very quickly, following a virtually linear curve. The force constant is larger and mechanical resonances shift to higher frequencies for higher bearing pressures (right hand graphs). The plot also shows the splitting of translational resonance positions, indicating that different conditions apply at opposite ends of the rotor. Part of the energy which is absorbed by the stator is proportional to the deviation of the rotor and thus to the imbalance. The eccentricity may become too large for the rotor-bearing geometry, or residual drive energy may become insufficient for a further rotor acceleration. Reduction of the force constant by lowering the bearing pressure brings resonance frequencies down and, by doing so sufficiently quickly, rotor motion may 'tunnel' beyond the critical resonance barrier. This procedure is frequently used to spin up poorly balanced rotors.

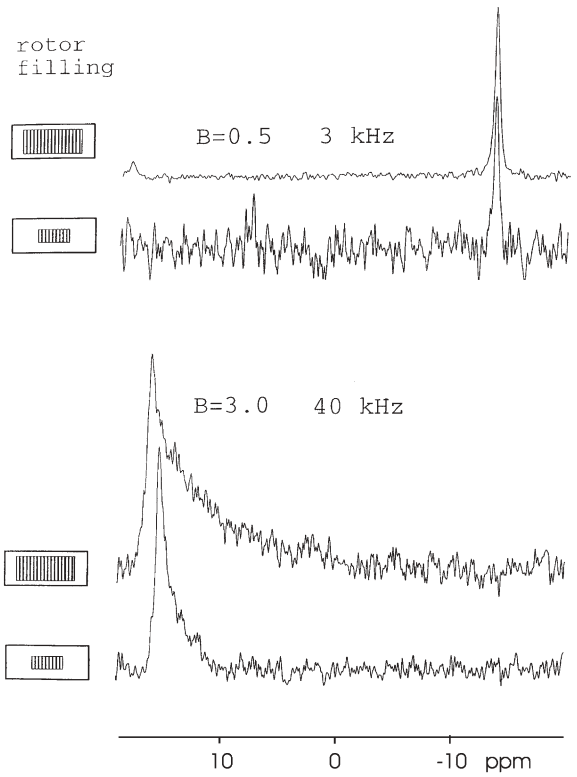

Fig. 2 ^{207}Pb signal of lead nitrate at 3 kHz and 40 kHz rotation frequencies. The profile of the signal reflects temperature distribution in the rotor, as tested with two filling configurations

Another common problem with fast rotation is rotor warming. Surface friction heats rotors proportionally to the second power of the speed [2]. Lead nitrate is a convenient compound to monitor the temperature via the change of chemical shift [3]. A peak shift of ca. 30 ppm, corresponding to a ca. 40 °C temperature increase, is observed as the rotation speed is increased to 40 kHz (Fig. 2). The distribution of the recorded signal is associated with the heating profile. This is a manifestation of the rotor size scaling. The ratio of the rotor surface area to the bulk volume scales up with the reduction of linear dimension, thus amplifying the temperature distribution. A very similar scaling effect applies to the inhomogeneity of the magnetic field induced by the coil and the stator. We have also observed a measurable increase in sample temperature in a poorly balanced rotor, indicating increased friction caused by reduction of the clearance between the rotor wall and the bearing surface. The spinning system is then more sensitive to other fluctuations, such as contamination of the driving gas by dust particles, and the probability of mechanical damage is thus increased.

3
Spectroscopy at High Speed Limits

One of the major problems in solid-state NMR is homogeneous line broadening of the spectra of abundant spin systems. Multiple-pulse suppression methods work only within a very limited range of rotation frequency and require extremely careful setup. Even then, results suffer from quantitative distortions by the frequency offset and by the relaxation and mobility properties of atoms at different positions within the solid. The offset and chemical shift anisotropy become even more of a problem at higher magnetic fields. A straightforward non-scaled Bloch decay measurement may be the most convenient and reliable solution in many cases. In addition, various 2D experiments benefit from direct suppression of the ^{1}H dipolar interaction. A combination of high rotation frequencies with increased chemical shift range at high magnetic fields is especially attractive [4]. While the homogeneous broadening remains constant on the frequency scale, line separation increases on the ppm scale. A "quadratic" effect can thus be obtained with a combined increase in mechanical spinning and in spin precession frequencies.

We have found that the dependence of the linewidth on rotor speed for the aminoacid alanine is almost linear (Fig. 3). Although the residual homogeneous dipolar line broadening is the dominant resolution-limiting factor even at 70 kHz, a much more detailed study of the individual lines and spin relaxation properties becomes feasible. For example, a rotation speed dependent relaxation has been observed and discussed by Gil and Alberti [5]. A site selective study will be available due to suppression of spin diffusion. Figure 3 also shows that the width of the lines from the amine protons converges to a quite different value than that from the aliphatic and methyl protons (see below).

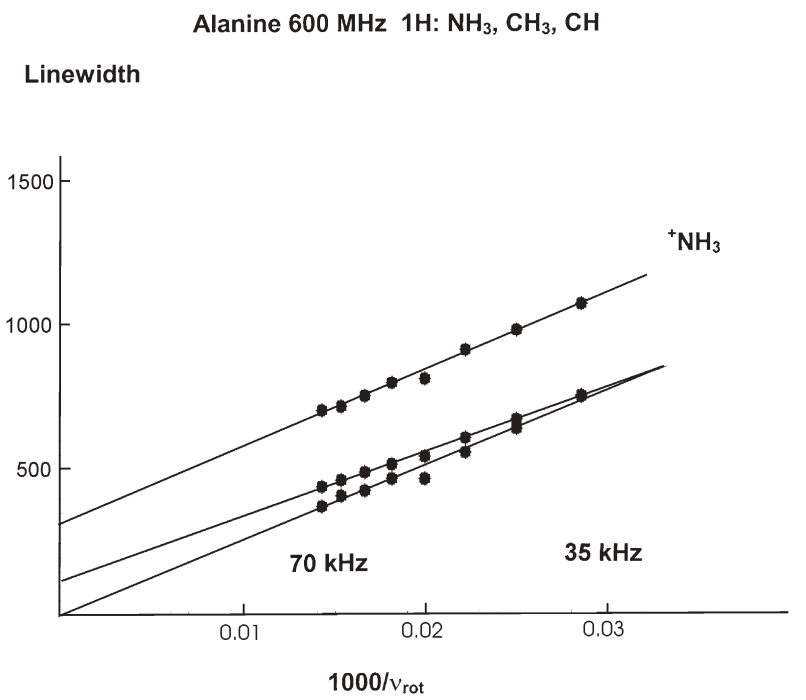

Fig. 3 Dependence of the linewidth of the ^{1}H spectrum of alanine on rotation speed, measured at 600 MHz. The sample was cooled to compensate for rotation-induced heating

Multi-spin behaviour in an abundant spin system can be observed indirectly by studying the linewidth dependence of a rare spin as a function of the amplitude of the decoupling radiofrequency. Figure 4 shows the efficiency of the proton decoupling on the amplitude of the alpha carbon line in glycine. Well known recoupling conditions, where the proton rf amplitude matches the double and single spinning frequency, are complemented by evidence of the recoupling at a third of the rotation frequency. This phenomenon becomes observable only at very high rotation frequencies (above 35 kHz) and implies a three-quantum overtone process in the proton spin system. Three-spin interactions have been theoretically analysed as the ultimate mechanism of homogeneous line-broadening at high rotation frequencies [6].

As is clear from Fig. 4, CW decoupling and resolution enhancement are more effective at the low end of decoupler power for a given range of ca 200 W. Low-power decoupling is a completely new situation in standard MAS. Theoretically, the order of spin interaction averaging is reversed, and mechanical reorientation has to be considered first. More sophisticated decoupling schemes have been proposed and analysed by Ernst et al. [7, 8]. Although the CH_2 lines were still narrower at high decoupling powers, the low power option constitutes a very competitive, if not better, alternative for the rest of the spectrum. In the

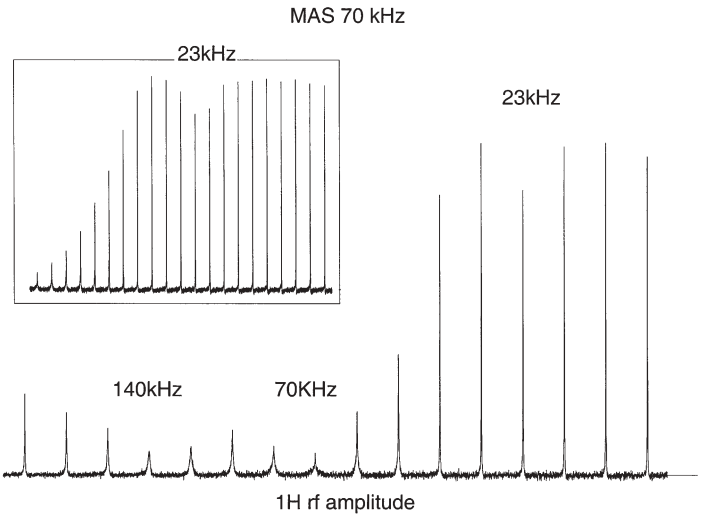

Fig. 4 Sequence of 150 MHz Cα lines of glycine with progressively decreasing decoupling power, step –1 dB and –0.25 dB (*insert*). Rotational resonances occur at double, single and fractional (1/3) rotation frequency

case of temperature-sensitive biological samples, low power decoupling may well become established as the method of choice.

Various correlation and internuclear distance measurements are based on zero- or double quantum spin flips. The most efficient correlation methods are based on the adiabatic process, which is relatively insensitive to actual, orientation-dependent coupling strength. A double-quantum spin flip is generated by a sweep of the rf field amplitude, centred at half rotation frequency (the HORROR condition [9]). The increased rotation frequency leads to a crucial improvement in the broad-band character of the DREAM method [10]. The zero-quantum adiabatic spin flip process is considered in the next section.

Various 1D and 2D experiments related to first-order quadrupole broadening also benefit from the fast rotation frequency. For heavier nuclei, quadrupole interaction and chemical shift anisotropy averaging at higher speeds results in better focusing of signal intensity to the remaining rotation sidebands (Fig. 5).

4 Rotation Sweep

The recently introduced rotation sweep spectroscopy [11] is based on the realization that decreased rotor size provides acceleration proportional to the inverse cube of the rotor diameter

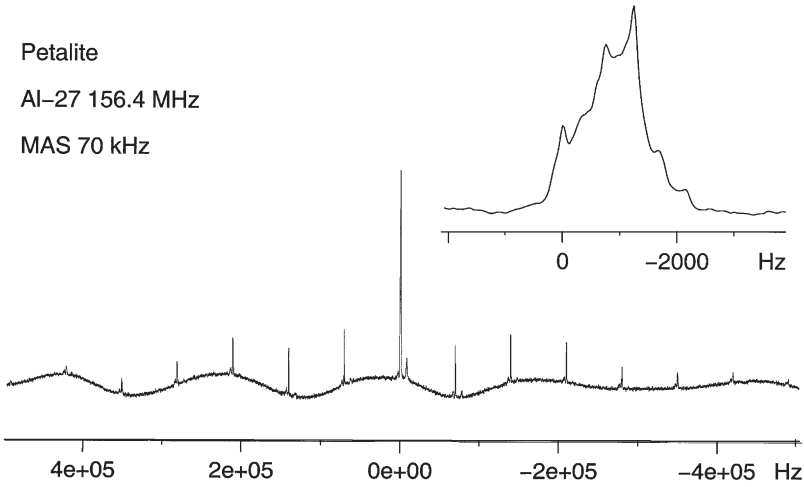

Fig. 5 ^{27}Al spectrum of the mineral petalite measured at 156 MHz. Quadrupole coupling can be estimated at 4.8 MHz, and the set of first-order satellite transition sidebands spans ca. 1 MHz

$$\dot{v} = \frac{16f}{\pi a \varrho} \frac{1}{D^3}$$

where, in addition to the definitions given earlier, f is the driving force per unit circumference. A stator with two 5-bar drive rings at opposite ends of the rotor provided acceleration rates up to 1 MHz for a 10 µL sample in our experimental setup. A rapid change of speed over 10 kHz is then performed in a timescale much shorter than typical spin-lattice relaxation, and even shorter than spin-lock relaxation in many cases. This experimental degree of freedom permits diverse real-time combinations of radiofrequency field amplitude and rotation frequency. For example, a robust broad-band cross-polarization approach was experimentally demonstrated [12]. Generally, efficient thermal contact between two spin species during sample spinning is provided only if the respective rf field amplitudes differ by a single or double rotation speed value. However, the rf field falls across the (regular pitch) solenoidal coil towards the coil ends in proportion to the maximum value, whereas spinning frequency is uniform. Therefore, whole sample cross-polarization is not possible if the two fields and sample spinning are kept constant. Fast acceleration is allowed to ramp the initially stationary sample to a regular high-resolution speed during the cross-polarization process. The resulting signal intensity is immune to variations of radiofrequency amplitude over the length of the coil and to a mismatch of the Hartmann-Hahn condition, thus providing maximum available polarization transfer over the entire sample.

A very useful class of solid-state experiments exploits the rotational resonance condition, where the rotation frequency is set to be equal to a multiple

of the difference between the isotropic line positions. Selective homonuclear recoupling is generated, providing information on the internuclear configuration. By changing the rotation speed, the rotational resonance condition can be passed adiabatically. A formal description can be given in terms of the interchange of phase (=identity) information of the two nuclear spins. The site-specific coherent phase, acquired during the evolution period, is stored in level population density matrix elements ϱ_{nn}. The sweep through the rotational resonance condition swaps populations ϱ_{11} and ϱ_{22} of the inner energy levels, which on the basis of the direct product can be written as:

$$M_{S1}(t) = Tr\{S1_z\varrho(t)\} = \frac{1}{2}(\varrho_{00} + \varrho_{11} - \varrho_{22} - \varrho_{33}) \rightarrow M_{S2}(t) \tag{5}$$

$$M_{S2}(t) = Tr\{S2_z\varrho(t)\} = \frac{1}{2}(\varrho_{00} + \varrho_{22} - \varrho_{11} - \varrho_{33}) \rightarrow M_{S1}(t) \tag{6}$$

The physical picture of the experiment is analogous to the adiabatic passage in the rotating frame, as in the case of a strong Zeman field and a small perturbing transverse field, which is scanned over the resonance condition of a two-level system by changing the carrier frequency. Here, a two-level system is composed of the inner pair of energy levels of a two-spin system, and the radiofrequency field is formed by the perpendicular component of a dipolar field, modulated by the sample rotation at the 'radio frequency', typically in the range of 10 kHz. If the rotation frequency approaches the difference between the energy levels, here equal to the difference in chemical shifts, spins start to follow the change of the dipolar field modulated by the rotor frequency sweep. An alternative description uses the avoidance of level crossing of the so-called dressed states [13], where each spin energy level is flanked with a swarm of virtual levels, displaced by multiples of the rotation frequency.

Unlike correlation spectroscopy based on spin diffusion, the adiabatic version enables, in principle, almost full exchange of magnetization between the two spins. As a result, the entire signal intensity will reside in the cross-peaks. Violation of the adiabaticity is characterized by the appearance of a diagonal peak and can be expected to occur if the rotation sweep is too fast compared to the interaction between spins. While numerical simulations indicate possible linear dependencies of the polarization transfer coefficient on spin coupling and the rate of the sweep over a range of practical values, the validity of this assumption remains to be tested. Here we present a semi-quantitative example of a relayed polarization transfer process.

The model test sample is uniformly ^{13}C enriched *trans*-crotonic acid. The methyl (S1) resonance is well separated from the two carbonyl lines. The closest carbonyl, S2, is spatially two bonds away, while S3 is directly bonded (Fig. 6). The usual spin phase encoding is stored after t_1 evolution in the z direction, whereupon the rotation speed is changed to sweep, in this case sequentially over the rotational resonance between methyl and both carbonyl sites. The mixing flowchart is thus composed of a sequence of passing rotational resonance

conditions. Assuming an initial rotation speed of ca. 10 kHz, which is then increased, the first contact is made between S1 and S2. For the sake of generality, only part of the exchange is expected. Once the frequency of rotation has reached 13–14 kHz, position S2 is labelled dominantly by the phase of S1. Since the distance is two bonds, the adiabatic condition may not be completely fulfilled and some residual original S2 phase is left on S2 too. Position S1 acquires phase information from S2 (plus some residual S1) in a complementary fashion. The next event is the exchange between S1 (which now actually carries new

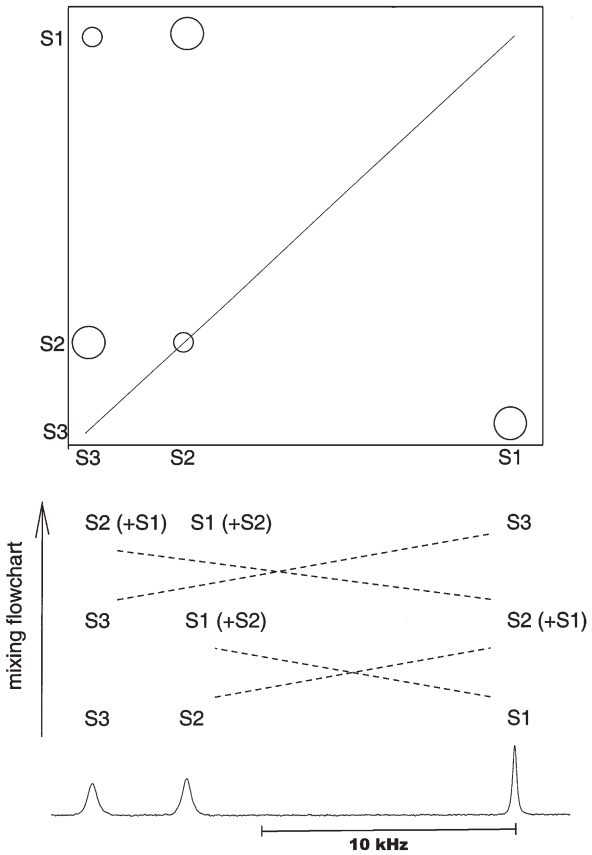

Fig. 6 Schematic presentation of events during a rotation sweep. The mixing flowchart presents a two-step relayed mixing process. Original populations along F_1 in sites S_3, S_2 and S_1 end up in positions as shown in *the top line*. The *rectangle* presents the resulting 2D spectrum, where original populations project to F_1 and final populations to F_2. 2D correlation is derived from labels of mixing flowchart top line (F_1 coordinate) and positions (F_2 coordinate). The relayed process of semi-adiabatic polarization transfer renders the cross-peak pattern asymmetric about the diagonal. The *bottom figure* represents the 1D spectrum of transcrotonic acid as a reference. The sideband of S_1 crosses the positions of S_2 and S_3 during the rotation sweep described

information from S2!) and S3. Here we assume full adiabatic exchange as a reflection of the much stronger one-bond dipolar interaction of the model sample. As a result, the two-dimensional spectrum shows migration from the original Sn positions (F1 dimension) to new locations. The signal from S3 resides at S1 in the final F2 dimension, S1 (+S2) at S2, and S2 (+S1) at S3. This is shown schematically by respectively larger and smaller circles in an illustrative 2D plot. The relayed transfer is characterized by a single cross-peak, i.e. a peak on one side of the diagonal only. Assigning transfer coefficients, *Kmn*, to the various rotational resonance exchange processes, a simple equation cascade can be written as

$$Sm_{i+1} = KmnSn_i + (1 - Kmn)Sm_i \tag{7}$$

The dynamics of the rotor speed can be conveniently analysed and adjusted by feeding a signal from the rotor motion monitor (via an optical fibre) to a console ADC (Fig. 7). The corresponding spectra are shown in Fig. 8. The faster sweep clearly reduces K12, and to a lesser extent K13. Both direct complementary peaks (1–Kmn) and relayed peaks depend on the product of complementary transfer coefficients, and correlate well with the expected influence of the sweep rate variation. The observed relay process can be shorted by proton-driven spin diffusion. Consequently, efficient rotation-speed independent (or carefully synchronized) decoupling is required during the entire mixing period.

The ^{13}C spectra of proteins consist of three separate bands, with the backbone carbons separated by 15–20 kHz in medium-field spectrometers, thereby enabling NMR sequencing of small peptides. On passing through rotational resonances in the aliphatic region, the carbonyl carbon will transfer magnetization from one adjacent α-carbon to the other, generating correlation peaks between sequential aminoacids. Figure 9 shows the results of NMR "Edman degradation" [14], where aminoacid sequencing can be directly inferred from the spectrum of a small model peptide.

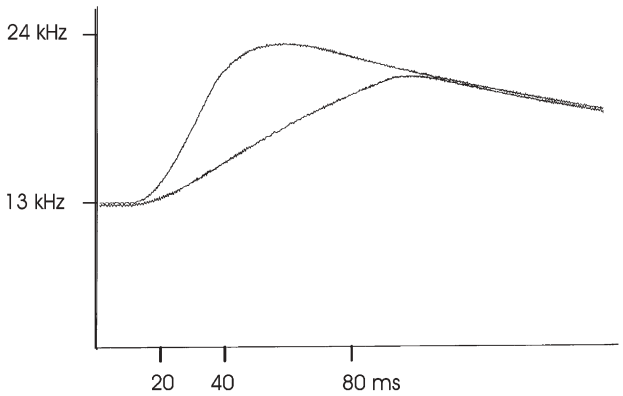

Fig. 7 Rotor speed profile for the two experiments in Fig. 8

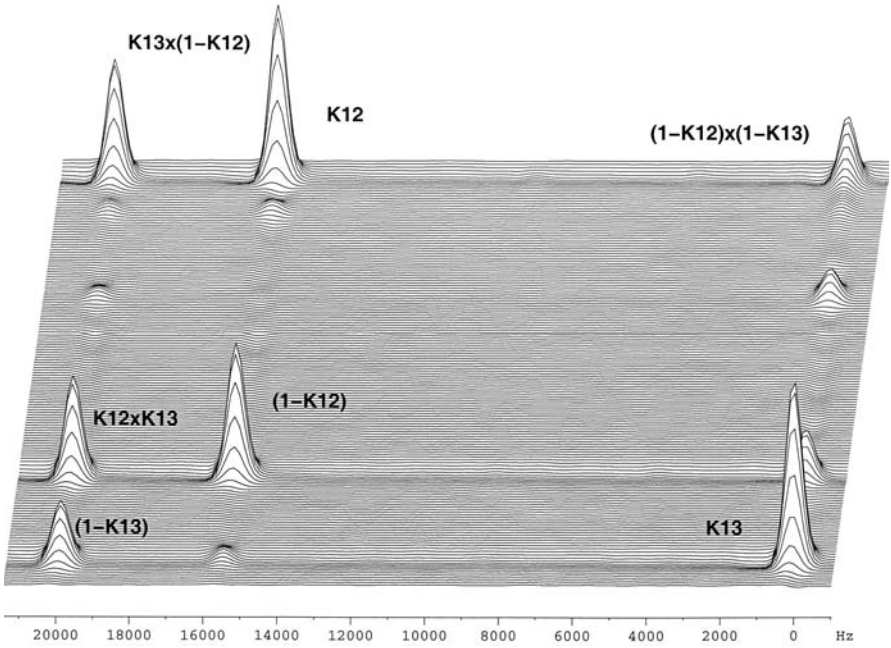

a

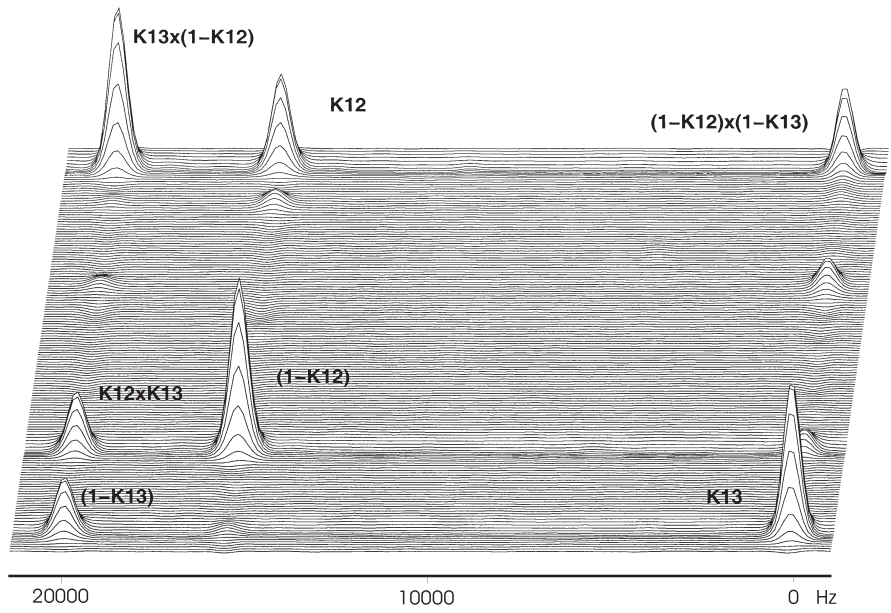

b

Fig. 8 Rotation sweep spectra of *trans*-crotonic acid at two different sweep rates

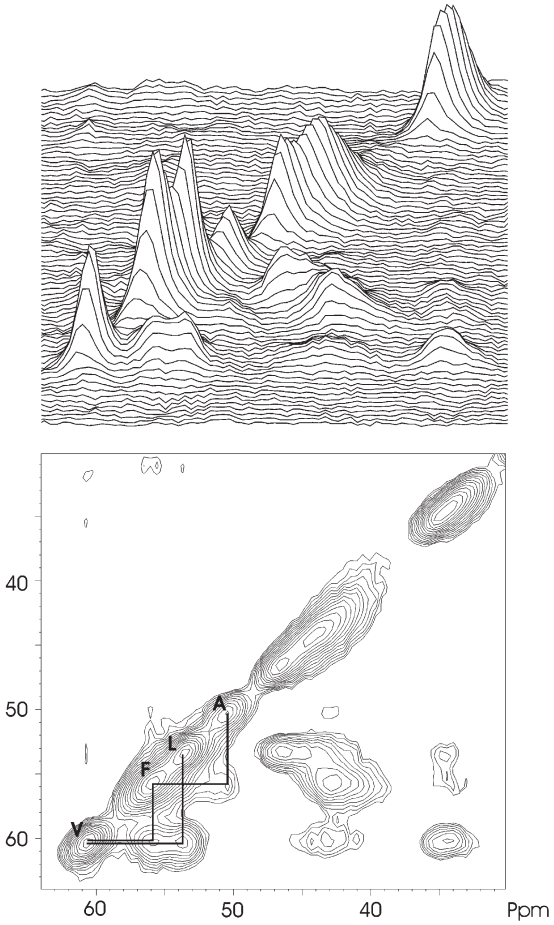

Fig. 9 NMR peptide sequencing by rotation sweep illustrated with a ^{13}C spectrum of the fully isotopically labelled peptide LVFFA. Carbonyl sites mediate polarization transfer between neighbouring alpha-carbons. The sequential ordering of amino acids can be directly inferred from the spectrum

5
Cryo-MAS™ [1]

The new potential of MAS comes mainly from a reduction in rotor size. The fastest rotors (70 kHz rotation frequency) currently hold 4 µL of sample, while ca. 10 µL samples can be rotated up to 50 kHz. If the filling factor is maintained, down-scaling leads to better mass sensitivity. On the one hand, increased mass sensitivity is welcome in cases where the availability of the sample is a problem,

[1] CRYOMAS is a registered trademark (NICPB, Tallinn, Estonia, 2004)

as is the case with isotopically labelled biopolymers. In addition, reduced rotor dimensions enable the construction of more efficient radiofrequency circuits at high frequencies. On the other hand, the absolute sensitivity decreases with the decreasing number of resonating nuclei. This disadvantage can be compensated for by working at lower temperatures. The effect of radiofrequency noise reduction has been exploited by using cryoprobes from high-resolution NMR (a term invented to annoy solid-state NMR spectroscopists), where the radiofrequency circuit is carefully isolated from the sample and cooled to ca. 20–30 K. A three- to fourfold improvement in the signal-to-noise ratio has been reported by commercial manufacturers. The same idea works much more effectively in solid-state NMR, since the sample generally does not need thermal isolation, being typically "frozen" already. Considering both major contributions, the increase in equilibrium magnetization and the reduction in thermal noise, a gain in sensitivity of an order of magnitude can already be expected at ~70 K. The theoretical factor of 30 in the signal-to-noise ratio can be reached when the temperature is reduced from 293 K to 30 K. The ideal gain, however, may be reduced by instrumental factors as well as by long relaxation times, if relaxation agents are not used.

Such obvious benefits have stimulated solid-state MAS experiments at cryogenic temperatures in several research laboratories. In the most successful and reproducible case, a sealed sample with a liquid-nitrogen temperature spinning module was cooled in a helium bath, but rotation speeds did not exceed 2 kHz at 40 K and 1 kHz at 5 K [15]. This is a serious limitation for practical applications.

The design features of the cooling technique harmonize perfectly with the general down-scaling. The requirements for lubrication and drive gas refrigeration power will be far less demanding, as will the thermal isolation of the probehead. The combined effect on power of heat extraction is thus very nonlinear. Moreover, the small mass of the sample enables the use of fast temperature ramps. Correlation spectroscopy of phase transitions and polarization enhancement using the Haupt effect [16], where dynamic proton polarization upon a rapid change of temperature is induced by the relaxation of the coupled nuclear spin and the methyl group rotation levels, are among potential applications.

Our prototype experiment, capitalizing on the new generation of fast rotors, demonstrated a promising perspective. At the lowest temperature, a 10-µL rotor was driven by helium gas at a rate of 3 m^3/h, cooled to 7 K by a heat exchanger located in the probehead. The heat exchanger was cooled by liquid helium at ca. 2–3 l/h. The temperature was measured by a thermometer in the exit gas flow. The rotor heating in the He atmosphere was controlled to within a few degrees. For a given rotor speed, the lowest temperature is determined mainly by the effectiveness of the heat exchanger. 7 K can be reached at 5 kHz, 13 K at 10 kHz, and 20 K at 20 kHz sample spinning. As an example, Fig. 10 shows the freezing of a H_2 molecule in a fullerene cage [17, 18].

The principal resolution may depend on the sample temperature. Understanding the interference of molecular motion with rotation and line narrow-

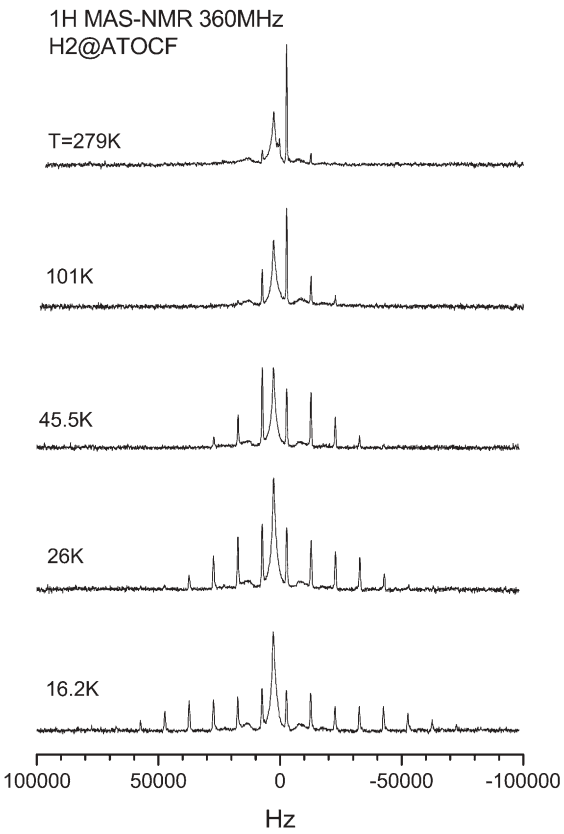

Fig. 10 Variable-temperature ^{1}H MAS spectra of H_2@ATOCF at 360 MHz, 10 kHz sample spinning speed. The spectrum at 279 K consists of a broad line from the protons at the fullerene opening region and of a sharp line corresponding to the hydrogen molecule which is rotating nearly freely inside the fullerene cage. The span of spinning sidebands is caused by the residual dipolar interaction between the protons of the hydrogen molecule. Below 100 K the sideband pattern broadens with decreasing temperature. Saturation of this broadening below 20 K indicates the freezing of the molecular rotation. The sample was synthesized by K. Komatsu and brought to our attention by M. Levitt and M. Carravetta

ing is essential for the design of multi-pulse line-narrowing techniques. In the case of alanine, reducing the temperature by ca. 50 K resulted in a significant broadening of the ^{1}H line from the amino group (higher field and higher rotation speed, Fig. 11). Measurements in a wide-bore magnet at lower temperatures confirm the broadening. Although the resolution is much lower because of the lower field and lower rotation speed, a reversal of the line-broadening effect could still be observed at the lowest temperature of 27 K. The central band and sidebands sharpen up, indicating different relative dynamics of the molecular motion. This phenomenon may also explain the failure of certain pulse narrowing techniques to maintain quantitatively correct intensity ratios of dif-

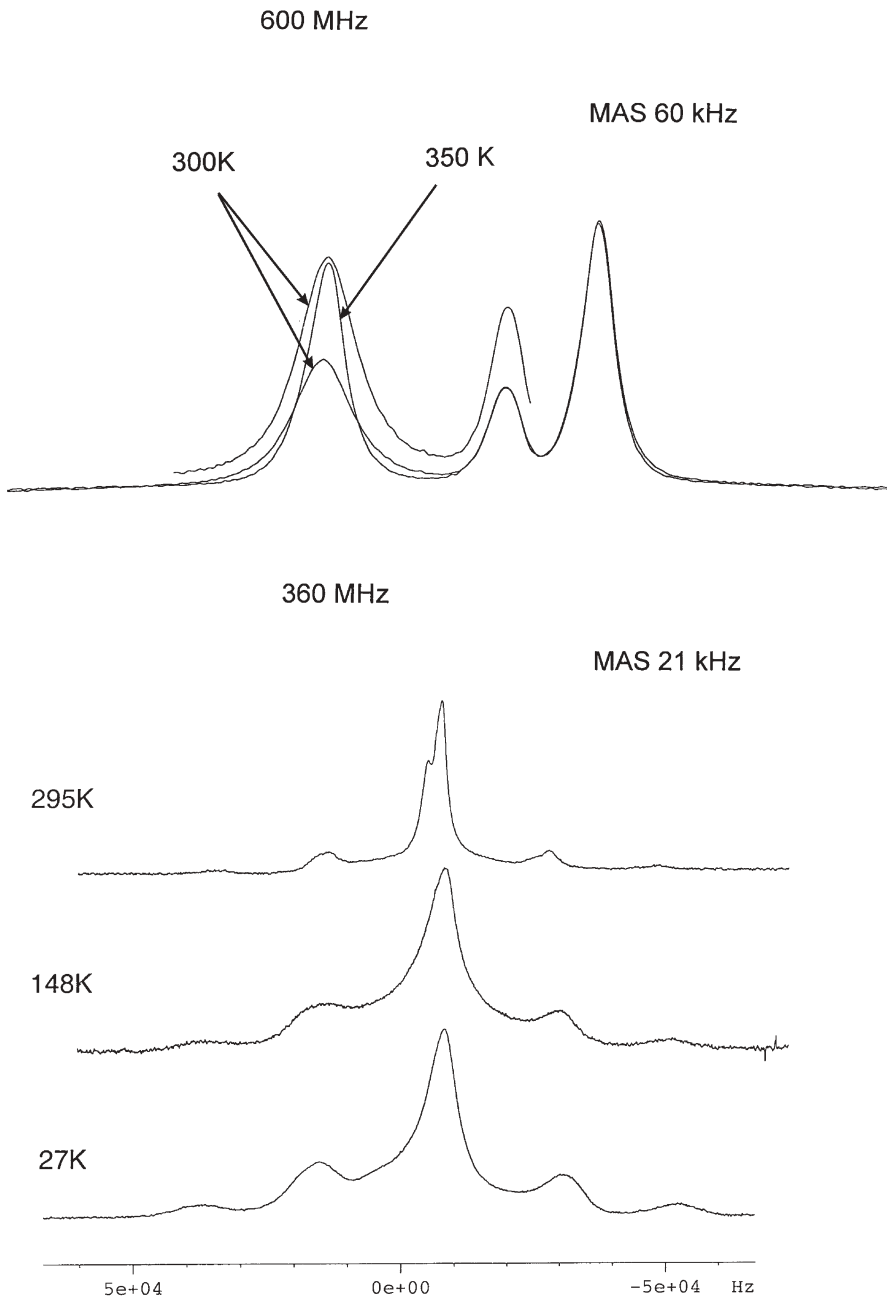

Fig. 11 Variable-temperature ^{1}H MAS spectra of alanine at 600 and 360 MHz. Low temperature spectra are registered for instrumental reasons at lower field; nevertheless sharpening of the signal can be observed at the lowest temperature

ferently moving molecular units and different convergences of linewidth on increasing rotation speed (Fig. 3).

6 Conclusions

Reduction of the rotor size opens up several hitherto unexplored avenues for study of the principles of MAS NMR and for practical applications. Exploitation of these new possibilities and features may sometimes reward the observant investigator with unexpected associations and nodes of seemingly unrelated regularities.

Acknowledgment This work was supported and encouraged by the Estonian Science Foundation and by collaborators at ETH Zürich, NHMFL, SUNY Stony Brook, and the Universities of Leipzig, Nijmegen and Warwick.

References

1. Samoson A (2002) Extended magic-angle spinning. In: The encyclopedia of nuclear magnetic resonance, vol 9. Advances in NMR. Wiley, pp 59–64
2. Geropp D (1969) Ing-Arch 38:195
3. Bielecki A, Burum DP (1995) J Magn Reson A116:215–220
4. Samoson A, Tuherm T, Gan Z (2001) Solid State NMR 20:130–136
5. Gil AM, Alberti E (1998) Solid State Magn Reson 11:203–209
6. Filip C, Filip X, Demco DE, Hafner S (1997) Mol Phys 92:757–771
7. Ernst M, Samoson A, Meier BH (2001) Chem Phys Lett 348:293–302
8. Ernst M, Samoson A, Meier BH (2003) J Mag Reson 163:332–339
9. Nielsen NC, Creuzet F, Griffin RG, Levitt MH (1992) J Chem Phys 9:5668
10. Ernst M, Meier MA, Samoson A, Meier BH (2004) J Am Chem Soc (in press)
11. Samoson A, Tuherm T, Past J (2002) Rotation sweep NMR. Chem Phys Lett 365:292–299
12. Samoson A, Tuherm T, Past J (2001) J Magn Reson 149:264–267
13. Shirley JH (1965) Phys Rev 138B:979
14. Edman P (1950) Acta Chem Scand 4:283
15. Myhre PC, Webb GG, Yannoni CS (1990) J Am Chem Soc 112:8991–8995
16. Haupt J (1972) Phys Lett 38A:389–390
17. Murata Y, Murata M, Komatsu K (2003) J Am Chem Soc 125:7142–7153
18. Carravetta M, Murata Y, Murata M, Heinmaa I, Stern R, Tontcheva A, Samoson A, Rubin Y, Komatsu K, Levitt MH (2004) Chem Soc (in press)